Journal of Biomedical Optics

BiomedicalOptics.SPIEDigitalLibrary.org

Quantification of endocytosis using a folate functionalized silica hollow nanoshell platform

Sergio Sandoval
Natalie Mendez
Jesus G. Alfaro
Jian Yang
Sharraya Aschemeyer
Alex Liberman
William C. Trogler
Andrew C. Kummel

SPIE.

Quantification of endocytosis using a folate functionalized silica hollow nanoshell platform

Sergio Sandoval,[a] Natalie Mendez,[b] Jesus G. Alfaro,[b] Jian Yang,[b] Sharraya Aschemeyer,[c] Alex Liberman,[b] William C. Trogler,[c] and Andrew C. Kummel[c,*]

[a]University of California, San Diego, Moores Cancer Center, Department of Bioengineering, CalIT^2 Nanomedicine Laboratory, La Jolla, California 92093, United States

[b]University of California, San Diego, Department of Nanoengineering, Chemical Engineering, and Material Science, La Jolla, California 92093, United States

[c]University of California, San Diego, Department of Chemistry and Biochemistry, La Jolla, California 92093, United States

Abstract. A quantification method to measure endocytosis was designed to assess cellular uptake and specificity of a targeting nanoparticle platform. A simple *N*-hydroxysuccinimide ester conjugation technique to functionalize 100-nm hollow silica nanoshell particles with fluorescent reporter fluorescein isothiocyanate and folate or polyethylene glycol (PEG) was developed. Functionalized nanoshells were characterized using scanning electron microscopy and transmission electron microscopy and the maximum amount of folate functionalized on nanoshell surfaces was quantified with UV-Vis spectroscopy. The extent of endocytosis by HeLa cervical cancer cells and human foreskin fibroblast (HFF-1) cells was investigated *in vitro* using fluorescence and confocal microscopy. A simple fluorescence ratio analysis was developed to quantify endocytosis versus surface adhesion. Nanoshells functionalized with folate showed enhanced endocytosis by cancer cells when compared to PEG functionalized nanoshells. Fluorescence ratio analyses showed that 95% of folate functionalized silica nanoshells which adhered to cancer cells were endocytosed, while only 27% of PEG functionalized nanoshells adhered to the cell surface and underwent endocytosis when functionalized with 200 and 900 μg, respectively. Additionally, the endocytosis of folate functionalized nanoshells proved to be cancer cell selective while sparing normal cells. The developed fluorescence ratio analysis is a simple and rapid verification/validation method to quantify cellular uptake between datasets by using an internal control for normalization. [DOI: 10.1117/1.JBO.20.8.088003]

Keywords: quantification; nanoparticle; endocytosis; targeting; confocal.

Paper 150289R received May 1, 2015; accepted for publication Jul. 27, 2015; published online Aug. 28, 2015.

1 Introduction

Diverse nanoparticle-based technologies are being developed for an array of biomedical applications, including drug delivery. These nanoparticles are typically synthesized using polymeric,[1–4] liposomal,[5–8] or inorganic formulations.[9–12] Most current cancer treatments do not greatly discriminate between cancerous and normal cells leading to systemic toxicity and adverse effects. Additionally, complete distribution into cancerous sites requires the administration of a drug in large doses, which further results in undesirable toxicity. Certain desirable attributes for nanocarriers are improved *in vivo* circulation, preferential accumulation and cellular uptake at target sites with minimal concentration in healthy tissues, and improved solubility, biocompatibility, and stability of therapeutic compounds.[13]

Many cancer therapeutics are hydrophobic drugs with poor bioavailability, solubility, and *in vivo* stability. As a result, these drugs are packaged with surfactants and other products which can have adverse side effects.[14] For therapeutics currently in development, such as siRNA, other nucleic acid based therapies, and catalytic enzymes, the *in vivo* half-life can be as short as a few minutes, therefore, a delivery vehicle is often necessary for increased effectiveness.[15–17] Encapsulation within a nanoparticle is one method being explored to aid in drug delivery.[18–23]

Elevated expression of the folate receptor (FR) occurs in many human cancers, which has led to the development of several folate targeting drug delivery systems.[24] Folate targeting has emerged as an attractive strategy for nanoparticle delivery due to: (a) the overexpression of FR α in a wide variety of human cancers including ovarian, breast, and colorectal cancers,[25–34] (b) FRs high-binding affinity for folic acid ($K_d \approx 0.1$ nM) and rapid internalization,[35] and (c) the decreased risk of folate targeted nanoparticles interacting with normal tissue. The few FRs that are expressed in normal cells are inaccessible from the circulation due to their location on the apical (i.e., lumen facing) surface of polarized epithelia.[36–38] Therefore, the overexpression and accessibility of the FR in many cancer cells suggests that it may be possible to concentrate a toxic dose to the diseased tissues while sparing the normal tissue from exposure to potent chemotherapeutics.[39]

A variety of methods have been studied to prepare targeted nanoparticles.[40–44] Folate targeting has been used to specifically target and deliver nanoparticles to a diverse range of cancers.[45–48] Several studies have shown effective folate targeting with silica,[49–51] gold,[52–55] iron-oxide,[12,56] liposome,[57–59] and polymer nanoparticles.[60–62] This work and several other studies suggest that cancer cells can be targeted with folate functionalized nanoparticles and used as effective drug delivery vehicles.[63–65]

*Address all correspondence to: Andrew C. Kummel, E-mail: akummel@ucsd.edu

1083-3668/2015/$25.00

Various techniques have been employed in quantifying cellular uptake and/or surface adhesion of nanoparticles. These techniques primarily involve quantification through fluorescence, mass, or atomic spectroscopy measurements.[66–70] Inductively coupled plasma-atomic emission spectroscopy (ICP-AES) and transmission electron microscopy (TEM) have been used in tandem to distinguish adhesion and internalization of gold particles into HeLa cells as a function of size, concentration, aspect ratio, and incubation time.[71] Fluorescence and confocal microscopy and ICP-AES spectroscopy have been used to quantify the uptake of superparamagnetic, folate/polyethylene glycol (PEG) functionalized magnetite particles in breast cancer and mouse macrophage cells.[45] The latter study found that functionalizing the surface of the particles with folate and PEG reduced protein adsorption and facilitated particle uptake. It is important to note that ICP-AES is not always an adequate technique to quantify intracellular uptake of magnetite nanoparticles due to endogenous iron present in cells which may introduce variability and poor reproducibility. Several of these techniques are frequently used in combination to quantify nanoparticle cell uptake and to distinguish particle adhesion to the cell surface from particle endocytosis. For example, in the study by Win et. al., the efficiency of targeted PLGA particle uptake in human colon adenocarcinoma cells was examined by detecting fluorescent markers with a fluorescence microplate reader, after performing multiple rigorous washing steps and lysing the plated cells. Subsequently, the data was confirmed qualitatively with confocal laser scanning microscopy, cryoscanning electron microscopy, and TEM to determine if the nanoparticles were internalized within cells[72] instead of adhering to the cell surface. One goal of the present study is to develop a simpler quantification method to measure endocytosis and to assess cellular uptake and specificity of a targeting nanoparticle platform. Hollow silica nanoshells were chosen for this investigation since they are of interest, as this platform can potentially be used to deliver a payload[73,74] that has been incorporated inside their hollow core, while leaving their surface free to be functionalized with a targeting ligand and/or a fluorescent reporter. A new fluorescence ratio analysis method is described. It was performed exclusively with the use of fluorescence and confocal microscopy images in order to quantify and differentiate between nanoparticle cell adhesion and intracellular uptake of 100-nm hollow silica nanoshells functionalized with folate. This was made possible with an internal standard for normalization and validation. To our knowledge, this is the first time that a simple fluorescence ratio analysis to quantify endocytosis using confocal microscopy has been described.

2 Experimental

2.1 *Materials*

Tetramethyl orthosilicate (TMOS), (3-aminopropyl)-triethoxysilane (APTES), *N*-hydroxysuccinimide (NHS), *N*-(3-dimethylaminopropyl)-*N′*-ethylcarbodiimide hydrochloride (EDAC), dimethyl sulfoxide (DMSO), and folic acid were obtained from Sigma–Aldrich (St. Louis, Missouri). Monomethoxypoly (ethylene glycol)-carboxymethyl (mPEG-CM, 2000 MW) was purchased from Laysan Bio (Arab, Alabama). The 100-nm amine functionalized polystyrene (APS) beads (2.5% w/w) were purchased from PolySciences Ltd (Warrington, Pennsylvania). HeLa cervical cancer cells and human foreskin fibroblast (HFF-1) were purchased from ATCC (Manassas, Virginia); Dulbecco's phosphate buffer saline solution (DPBS 1×) and fetal bovine serum (FBS) were purchased from Mediatech, Inc. (Manassas, Virginia). RPMI 1640 folate free medium, media supplements, Hoechst 33342, wheat germ agglutinin (WGA), fluorescein isothiocyanate (FITC), Prolong Gold, and CellTracker CMFDA green, CellTracker CMAC blue, CellTracker CMPTX red intracellular stains were obtained from Life Sciences Corporation (Carlsbad, California). Nunc Lab-Tek II 4-well chamber slides and paraformaldehyde (PFA) were purchased from ThermoFisher Scientific (Fair Lawn, New Jersey). All chemicals and reagents were used as received or as described in manufacturer protocols unless otherwise stated.

2.2 *Preparation of Hollow Silica Nanoshells*

Silica nanoshells were prepared using a previously reported method.[10,74,75] Briefly, this was accomplished by taking APS beads (100 μl, 2.5% w/w) and suspending them in absolute ethanol (1.75 mL). TMOS (6.5 μl) was added to this suspension. The mixture was stirred with a vortex mixer at room temperature at a speed of 900 rpm. After 12 h of stirring, a white precipitate was collected by centrifugation, washed with ethanol, and dried in vacuum for 48 h at room temperature to give 4.1 mg of core-shell spheres. The APS core was removed by calcining the 4.1 mg of core-shell nanoshells by heating in air at 5°C per minute to 500°C and maintaining this temperature for 24 h. About 1.5 mg of hollow SiO_2 nanoshells were collected as a white powder.

2.3 *Preparation of NHS-Folate and NHS-mPEG*

Active intermediate *N*-hydroxysuccinimide-folate (NHS-folate) was synthesized by adding NHS (0.94 mg), EDAC (1.57 mg), folic acid (3 mg), and DMSO (1 mL) in a 2-mL Eppendorf tube. This mixture was vortex mixed at 3000 rpm for 24 h and used within 24 h to functionalize nanoshell surfaces with folate. Similarly, *N*-hydroxysuccinimide-mPEG (NHS-mPEG) was prepared by weighing out NHS (0.94 mg), EDAC (1.57 mg), and mPEG (13.6 mg, molar equivalent to 3 mg of folic acid) in an Eppendorf tube. Contents were suspended in 1 mL of DMSO, and the mixture was vortex mixed at 3000 rpm for 24 h. The final solution was used within 24 h to prepare non-targeted PEG functionalized nanoshells.

2.4 *Amine Surface Functionalization of SiO_2 Hollow Nanoshells with APTES*

Before functionalizing nanoshell surfaces with FITC, NHS-folate, and/or NHS-mPEG, nanoshells had to be first amine functionalized. This was accomplished by suspending particles (3 mg) in a solution composed of ethanol (1 mL) and APTES (0.3 μL) in a 2-mL Eppendorf tube. The suspension was stirred for 2 h and the nanoshells were collected by centrifugation, washed twice with ethanol, and resuspended in DMSO (1 mL).

2.5 *Surface Modification of SiO_2 Hollow Nanoshells with FITC and NHS-Folate or NHS-mPEG*

In a 2-mL Eppendorf tube containing amine functionalized nanoshells (3 mg) suspended in DMSO (1 mL), FITC solution (2 μL of 10 mg/mL in DMSO) was added to the particles in parallel with a variable amount of a NHS-folate or NHS-PEG solution in DMSO. The variable amounts of NHS-folate

solution contained either 2, 20, or 200 μg of NHS-folate, while variable amounts of NHS-PEG solution contained 9, 90, or 900 μg of NHS-PEG. These nanoshell solutions were vortex mixed for 24 h at 3000 rpm. After mixing, the particles were washed twice with DMSO and resuspended in PBS (1 mL) for use in cell experiments.

2.6 *Characterization of Functionalized SiO_2 Hollow Nanoshells*

Scanning electron microscopy (SEM) analysis of nanoshells was conducted on a FEI/Philips XL30 FEG ESEM microscope with an accelerating voltage of 10 kV. TEM analysis of nanoshells was conducted on a Sphera 200 kV instrument equipped with a LaB_6 electron gun, which uses a standard cryotransfer holder developed by Gatan, Inc. A Zetasizer Nano ZS (Malvern Instruments) was used to measure the dynamic light scattering (DLS) size distribution, polydispersity index, and zeta potential of nanoshells suspended in distilled water (3 mg/mL), and after 3 h of alternating 15 min periods of gentle sonication and vortex mixing.

Quantification of the maximum amount of folate on nanoshell surfaces was performed on nanoshells functionalized only with NHS-folate. During particle functionalization, supernatants from the wash steps were collected and analyzed by UV-Vis spectrophotometry (Perkin Elmer Lambda Scan 35). To calculate the amount of folate retained by the particles, the absorbance peak at $\lambda = 350$ nm, which is also observed by other groups,[76–78] was converted into a concentration and multiplied by the volume of the washes resulting in a known mass of folate which was not conjugated onto the particle. This mass was subtracted from the known starting mass of the folate added to the particles during the synthesis reaction to calculate the amount of folate on the surface of the total particles. Using a previously reported weight factor equation method,[74] an estimate of the number of nanoshells used in the synthesis reaction was calculated along with the amount of folate actually present on the surface of the total particles, to determine the average value of folate molecules per nanoshell.

Incorporation of FITC on nanoshell surfaces was evaluated using fluorescence spectroscopy analysis. Fluorescence intensities were measured using a Tecan Infinite M200 microplate reader at an excitation λ of 490 nm and an emission λ of 520 nm. Nanoshells were suspended in PBS at a particle concentration of 20 μg/ml and were measured in triplicate.

2.7 *Cell Culture—HeLa Cells Only Samples*

HeLa cervical cancer cells were grown at 5×10^4 cells/well on Nunc Lab-Tek II 4-well chamber slides in RPMI 1640 folate free medium supplemented with 10% FBS and 1% antibiotics (penicillin, streptomycin, glutamine) at 37°C in a humidified atmosphere of 5% CO_2. Before starting cell adhesion/endocytosis experiments, the cells were grown to 60 to 80% well confluency.

2.8 *Cell Culture—Nanoshell Selectivity Experiments*

Using 15-mL falcon tubes, HeLa and HFF-1 cells were individually stained in an RPMI 1640 folate-free complete media suspension (2 mL) following manufacturer guidelines. Briefly, HeLa cells were stained with CMPTX CellTracker Red intracellular stain (final concentration of 5 μM), while HFF-1 cells were stained with CMAC CellTracker Blue (20 μM) for 30 min while under gentle agitation using a Barnstead/Thermolyne Labquake rotisserie in order to prevent cells from adhering to falcon tubes. Cells were washed twice to remove excess dye and resuspended in RPMI 1640 folate free complete media. Since normal cells tend to grow at a slower pace than cancer cells, HFF-1 were mixed with HeLa cells at a 3:2 ratio before being plated on Nunc Lab-Tek II 4-well chamber slides in RPMI folate free complete media. Samples were incubated at 37°C in a humidified atmosphere of 5% CO_2 for 24 h to allow the cells to adhere to slide surfaces.

2.9 *Cell Adhesion/Endocytosis Experiments*

In order to determine the extent of nanoshell cell adhesion/endocytosis, HeLa cell samples were incubated with folate/FITC (100 μg/mL) or PEG/FITC (100 μg/mL) functionalized SiO_2 nanoshells for 24 h in RPMI folate free complete media at 37°C in a humidified atmosphere of 5% CO_2. Afterward, cells were washed twice with DPBS and labeled with WGA membrane stain (5 μg/mL) and Hoechst nucleus dye (0.01 μg/mL) in DPBS for 30 min. Subsequently, cells were washed 3× with DPBS to remove any excess dye, fixed with 4% PFA in DPBS solution, washed twice more with DPBS, and covered with Prolong Gold antifade reagent in order to prepare samples for visualization by fluorescence and/or confocal microscopy.

This protocol was adapted for the nanoshell selectivity experiments, with the notable exception of the staining step, as cells were prestained before cell plating in order to distinguish cell types, and incubating nanoshell concentrations were reduced to 50 μg/mL. Prestaining does not affect cell viability or proliferation as described by the manufacturer.

2.10 *Fluorescence Microscopy of Nanoshell Cell Adhesion*

Fluorescence microscopy was used to visualize the adhesion of folate/FITC or PEG/FITC functionalized SiO_2 nanoshells in adhesion/selectivity experiments. Three individual fluorescent images (blue, red, and green channels) were captured using a Zeiss AxioImager Z1 (Carl Zeiss Inc., Thornwood, NY) fluorescence microscope and a 1.4 mega-pixel Photometrics CoolSNAP HQ^2 camera with the appropriate color filter. The samples were imaged at 40× magnification and had an image resolution of 0.1566 μm/pixel. The green fluorescence images were visualized using a Zeiss 38HE filter set. Zeiss filter sets 49 and 32 were used to visualize the blue and red fluorescence, respectively. The resulting images were compiled and processed using ImageJ (NIH, Bethesda, Maryland). The excitation source was a short arc mercury lamp.

2.11 *Confocal Microscopy Studies of Nanoshell Uptake by HeLa Cells*

Confocal microscopy was employed to visualize the uptake of folate/FITC or PEG/FITC functionalized SiO_2 nanoshells by HeLa cervical cancer cells. Z-stack images were captured using a Zeiss LSM510 laser scanning microscope using a Plan-Apochromat 100× 1.4 NA oil objective lens. Sequential 90 μm × 90 μm (frame size 1024 × 1024) sections were acquired at 0.7 micron intervals in the z direction with excitation wavelengths of 364, 488, and 543 nm. The same microscope settings which include image acquisition and exposure times were used to eliminate additional variation. All samples,

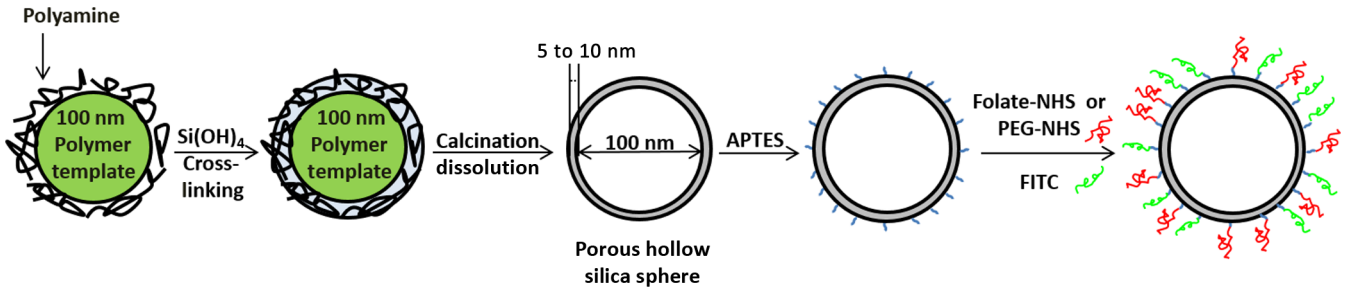

Fig. 1 Nanoshell synthesis and functionalization. 100-nm amine functionalized polystyrene beads were mixed with hydrolyzed tetramethyl orthosilicate which was used as a precursor for the silica shell. Polymer-core nanoshells were calcined at 500°C to form porous hollow silica nanoshells. (3-aminopropyl)-triethoxysilane was added for amine functionalization on the nanoshell surface. Active *N*-hydroxysuccinimide-polyethylene glycol (NHS-PEG) or NHS-folate was functionalized on the nanoshell surface along with fluorescein isothiocyanate (FITC).

including controls, were performed with the same antibody stock and the same cell passage.

3 Results and Discussion

3.1 *Characterization of Functionalized SiO_2 Hollow Nanoshells*

As shown in Fig. 1, hollow silica nanoshells were functionalized with 20 μg of FITC and varying amounts of NHS-folate or NHS-mPEG (PEG 2000 kDa), at 200, 20, 2, or 900, 90, 9 μg, respectively. Hollow silica nanoshells were used due to their broad range of applications and their growing interest in the field.[73,74,79] Hollow calcined silica nanoshells, which were used in the present study, have shown that they can remain intact in human serum up to 24 days and can be doped with iron to make them biodegradable.[80] Folate was used as a targeting ligand because FRs type α are frequently over-expressed in cancer cells. PEGylation typically decreases cell internalization,[81,82]

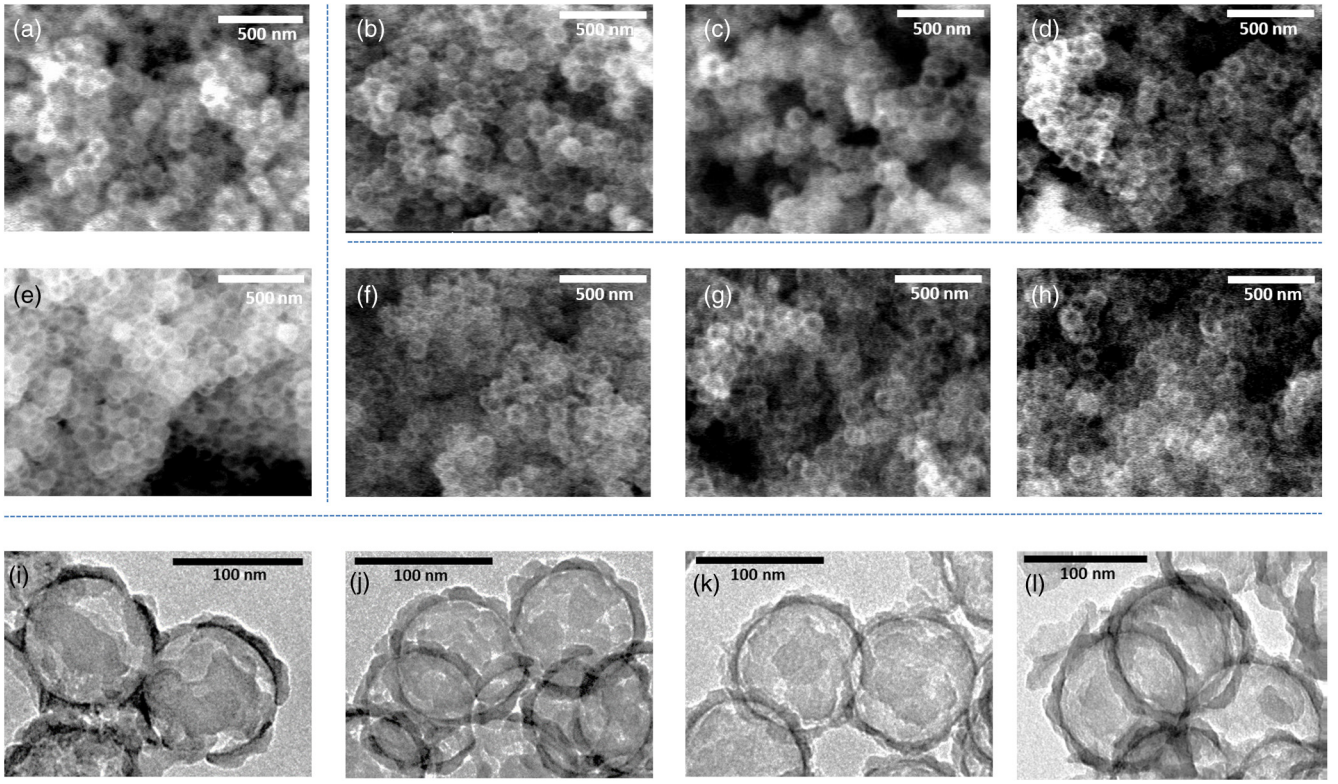

Fig. 2 Nanoshell characterization. Scanning electron microscopy (SEM) images show no morphological differences can be observed after surface modification by SEM analysis: (a) nanoshells (no coating), (b) 2-μg folate/20-μg FITC nanoshells, (c) 20-μg folate/20-μg FITC nanoshells, (d) 200-μg folate/20-μg FITC nanoshells, (e) 20-μg FITC nanoshells, (f) 9-μg PEG/20-μg FITC nanoshells, (g) 90-μg PEG/20-μg FITC nanoshells, and (h) 900-μg PEG/20-μg FITC nanoshells. All SEM images were taken at 36,000× magnification. (b) Transmission electron microscopy images of 100-nm nanoshells functionalized with FITC, folate, and/or PEG show no morphological differences after surface modification: (i) nanoshells (no coating), (j) 20-μg FITC nanoshells, (k) 200-μg folate/20-μg FITC nanoshells, and (l) 900-μg PEG/20-μg FITC nanoshells.

therefore, PEG nanoshells were used to compare low-internalizable particles to folate nanoshells which are highly internalizable. PEG was functionalized on the nanoshell surface at the same molar ratio as folate to nanoshells, in order to have molar equivalent nanoshell controls. Plain and functionalized nanoshells were characterized by SEM and TEM as shown in Fig. 2. All samples were verified to be round shaped hollow nanoshells with narrow size distributions. No significant morphological differences were observed after nanoshell surface modification. In addition, size distribution of nanoshells was quantified by measuring the diameter of nanoshells using TEM images. The average size ± SD of nanoshells are shown in Table 1.

For net surface charge characterization, electrophoretic light scattering was used to measure zeta potentials as shown in Table 2. The zeta potential measurements show that as nanoshells were functionalized with increasing amounts of PEG, the zeta potentials remained constant. Conversely, when nanoshells were coated with increasing amounts of folate, the nanoshell charge became increasingly more negative, probably due to the presence of more folate molecules on the surface of the nanoshells in their deprotonated folate carboxylic state, resulting in a greater net negative charge. This increase in net negative charge suggests that as folate is increased during the nanoshell functionalization step, the particles become more colloidally stable and more resistant to aggregation in water.

DLS was employed to measure the polydispersity of nanoshells and confirm consistency between particle batches (Table 2). The hydrodynamic diameter is not reported due to sample absorbance and fluorescence from the FITC and folate. The zeta potential measurements are less affected by optical distortion since it is based on measuring the electrophoretic mobility of particles.

FITC incorporation was measured in order to determine if the amount of FITC conjugated on the nanoshell surfaces was consistent for plain, PEG, and folate functionalized nanoshells. As shown in Fig. 3, SiO_2-FITC nanoshells had the most FITC incorporation. Nonetheless, all samples conjugated with FITC were within the same order of magnitude. For folate nanoshells, FITC conjugation was consistent at 2, 20, and 200 μg folate, whereas FITC incorporation was higher for PEG nanoshells at higher PEG concentrations. It is important to note that the fluorescence intensities for FITC-folate nanoshells were slightly lower than for plain nanoshells and nanoshells functionalized with PEG. These differences may be due to the surface area available for ligand attachment, competition, different chemical structures, and different local surface environment/pH which may alter the conjugation chemistry.

Table 1 Size characterization of nanoshells from transmission electron microscopy images. The diameters of nanoshells were measured for nonfunctionalized SiO_2 nanoshells, FITC-SiO_2, and FITC-SiO_2 nanoshells functionalized with 200-μg folate or 900-μg PEG. All particles show similar average sizes with a narrow size distribution.

Sample name	Nanoshell diameter (nm) ± SD	Count (n = number of nanoshells)
Nanoshells (No coating)	115 ± 6	149
20-μg FITC nanoshells	107 ± 7	92
200-μg folate/20 μg FITC nanoshells	112 ± 6	97
900-μg PEG/20-μg FITC nanoshells	115 ± 7	80

Table 2 Surface charge characterization of nanoshells using dynamic light scattering. Zeta potentials and polydispersity (PDI) of 100-nm noncoated SiO_2 nanoshells, FITC-SiO_2, and FITC-SiO_2 functionalized with folate or PEG were measured using DLS in Milli-Q water. Measurements show that nanoshells functionalized with more folate have a larger net negative charge. PDI was employed to confirm consistency and colloidal stability between the batches of particles.

Sample name	Zeta potential (mV)	PDI
Nanoshells (no coating)	−40	0.24
Silica (20-μg FITC) nanoshells	−6	0.46
2-μg folate/20-μg FITC nanoshells	−8	0.64
20-μg folate/20-μg FITC nanoshells	−14	0.53
200-μg folate/20-μg FITC nanoshells	−25	0.36
9-μg PEG/20-μg FITC nanoshells	−12	0.68
90-μg PEG/20-μg FITC nanoshells	−12	0.53
900-μg PEG/20-μg FITC nanoshells	−12	0.41

3.2 *Quantification of Maximum Amount of Folate on Nanoshell Surfaces*

The maximum amount of folate on nanoshell surfaces was estimated by using a previously reported weight factor equation [74] (See Appendix) and UV-Vis spectrophotometry to calculate the amount of folate conjugated on three different nanoshell batches after NHS-folate only functionalization. Any folate not present in the supernatant was assumed to be functionalized onto the nanoshells. As shown in Fig. 4, the results showed that as

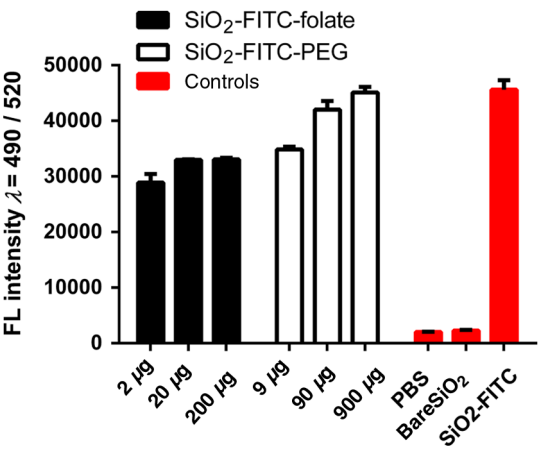

Fig. 3 Incorporation of FITC in silica nanoshells. Fluorescence intensities of FITC conjugated to the surface of SiO_2, SiO_2-folate, and SiO_2-PEG were measured at 490 nm/520 nm. Fluorescence intensity was greatest for SiO_2-FITC nanoshells. The fluorescence intensity of SiO_2-FITC-PEG nanoshells increased when PEG was increased from 9 to 900 μg. For SiO_2-FITC-folate nanoshells, FITC conjugation was consistent at 2, 20, and 200 μg folate.

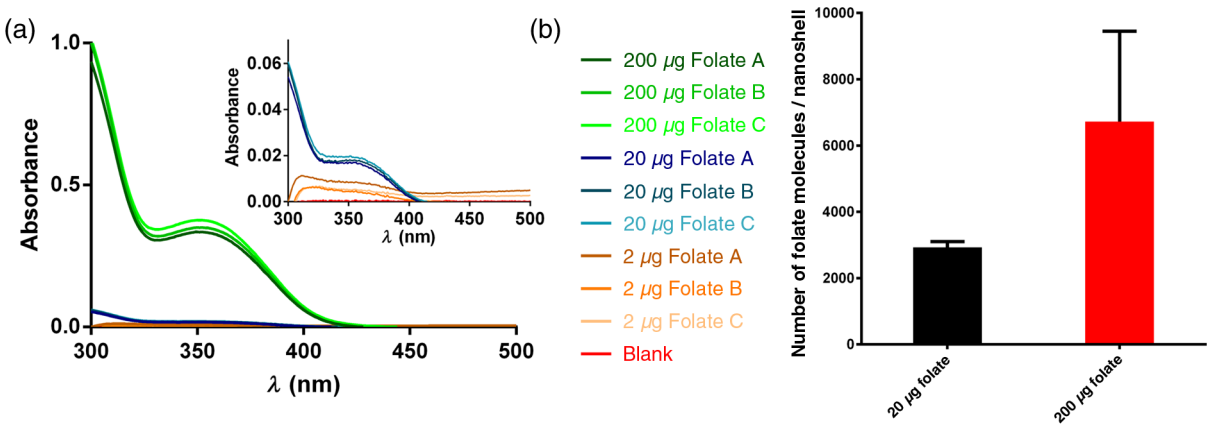

Fig. 4 Estimated maximum amount of folate molecules functionalized on nanoshell. Three different nanoshell batches were functionalized with 200, 20, or 2 μg of folate (No FITC). After nanoshell functionalization, supernatants of nonreacted folate were collected and analyzed with UV Vis. Folate not present in supernatant was assumed to be functionalized onto the surface of nanoshells. (a) UV-Vis at wavelength 350 nm was used to determine remaining nonreacted folate in solution. Insert is a zoom in to show the 350-nm peak of 20-μg samples. (b) Calculated average number of folate molecules functionalized on an individual nanoshell based on UV-Vis data.

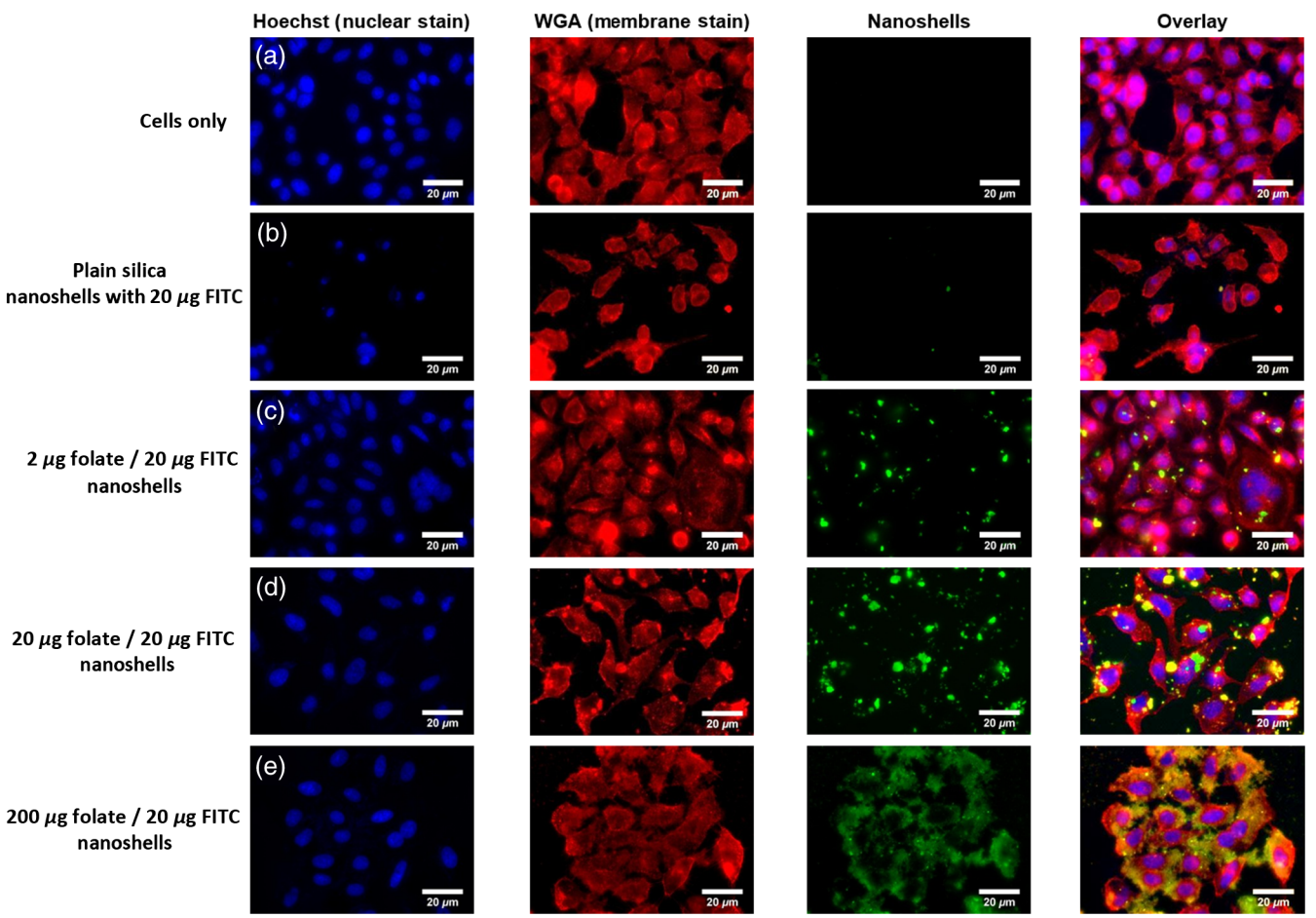

Fig. 5 Effect of SiO_2 nanoshells functionalized with folate on cellular adhesion/endocytosis by fluorescence microscopy. HeLa cells were incubated with nanoshells functionalized with 20-μg FITC and 0, 2, 20, or 200 μg folate. (a) HeLa cells stained with WGA membrane stain (red) and Hoechst nuclear stain (blue) with no nanoshells. HeLa cells incubated with 100 μg/mL of nanoshells functionalized with: (b) 20-μg FITC (green), (c) 2-μg folate/20-μg FITC, (d) 20-μg folate/20-μg FITC, or (e) 200-μg folate/20-μg FITC. Increase in green fluorescence around cells indicates increase in nanoshell adhesion/endocytosis.

more folate was added during the reaction step, more folate bound to the nanoshells. On average, over 6700 [standard error (SE) ± 1570] folate molecules were coated on each nanoshell when 200-μg folate was added to the reaction, but only 2900 (±97) folate molecules adhered to each nanoshell when 20-μg folate was added during the synthesis [Fig. 4(b)]. Taking into account that SiO_2 nanoshells are porous as determined by previous BET results,[79] it is highly probable that folate molecules could seep into the nanoshell interior surface areas, as well as the pore area in the shell wall. In order to account for this, the number of folate molecules was calculated using the BET data[79] and a weight factor equation (See Appendix), which suggest that about 14% of the folate molecules are present on the nanoshell outer surface, while the remaining folate molecules would cover the nanoshell inner surface and the shell pores within the shell wall, since only 14% of the total surface area is the outer surface area. The 2-μg sample calculations are not being reported because UV-Vis data for these batches were below detection levels.

3.3 *Nanoshell HeLa Cell Adhesion Experiments and Fluorescence Microscopy Image Analysis*

To evaluate the extent of target-specific cellular adhesion of folate functionalized nanoshells, FR overexpressing HeLa cancer cells were used *in vitro* and were studied and visualized using florescence microscopy. As shown in Fig. 5, incorporating a higher amount of folate on the nanoshell surface resulted in an increase of nanoshell binding to the surface of HeLa cells. Furthermore, at higher folate concentrations, the nanoshells adhering to the cell surface appeared more dispersed and formed a uniform coating around cells. Nanoshells with less folate on their surface tended to attach to cells in large bright clumps. HeLa cell samples were also incubated with low-internalizable PEG functionalized nanoshells and compared to their folate functionalized nanoshell molar equivalent counterparts. As shown in Fig. 6, HeLa cells incubated with nanoshells functionalized with increasing folate concentrations on their surfaces showed increasing cell adhesion as folate concentration increased [Figs. 6(a)–6(c)]; however, no increase in cell adhesion was observed with increasing PEG concentration [Figs. 6(d)–6(f)]. Similarly, plain silica nanoshells with FITC [Fig. 6(g)] showed little to no particle adhesion.

In order to quantify and confirm that these green particle-like features were due to the adhesion of nanoshells and not an optical artifact, a modified version of a previously reported fluorescence ratio analysis[83] was performed on cell outlines using the individual red and green channel images. Briefly, using Image J, cytoplasmic cell outlines were created to measure the extent of nanoshell adhesion on cells. If there was significant contact between neighboring cell membranes, those cells were excluded from analysis. If cells came into some contact, the boundaries of the cells were outlined without overlapping. The cell outlines were based on the individual red channel images and were applied to the same location/coordinates on their green channel counterparts by using the ROI manager in Image J. The Image J analyze/measure tools were used to determine the mean fluorescence values inside the cell outlines for both the green and red channels, which in turn were used to calculate the fluorescence ratio, i.e., mean green fluorescence divided by mean red fluorescence, of each outlined cell. Division by the mean red fluorescence intensity of each cell outline was used as an internal control in order to allow for the comparison of corresponding normalized values for different datasets. Hereafter, fluorescence ratio will be defined as the mean green fluorescence intensity divided by the mean red fluorescence intensity (FL I) of each cell outline. Several approaches were considered in order to determine the best quantification method including mean green FL I/ROI area, mean green FL I/mean blue FL I, and IntDen green FL I/red FL I, however, we found that the best method was mean green FL I/mean red FL I applied with a

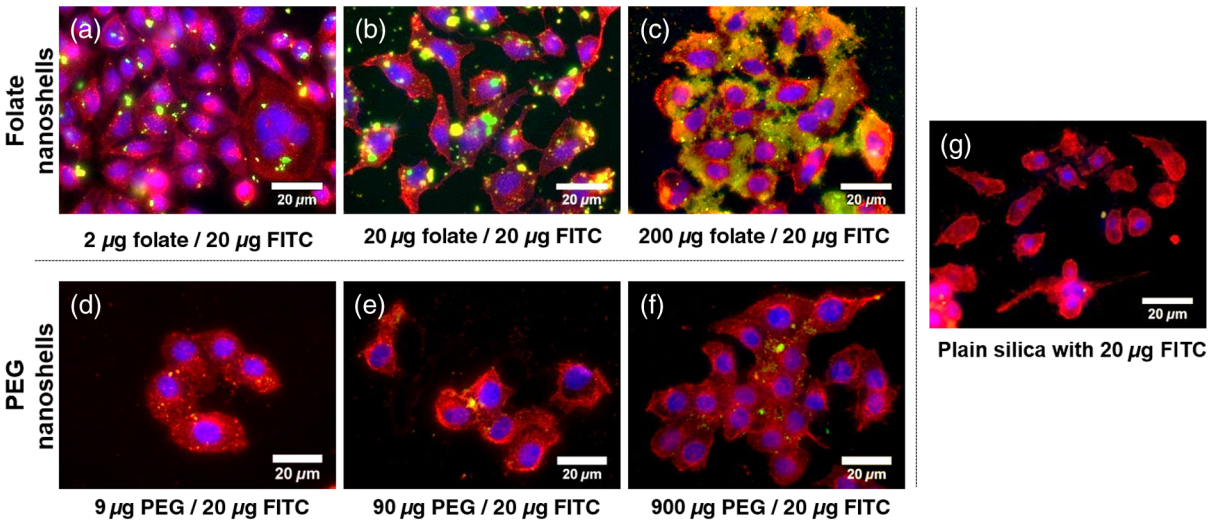

Fig. 6 Comparison of plain silica, folate targeted, and PEG nanoshells cell adhesion/endocytosis by fluorescence microscopy. HeLa cells were incubated with 100 μg/mL of targeted nanoshells functionalized with: (a) 2-μg folate/20-μg FITC, (b) 20-μg folate/20-μg FITC, or (c) 200-μg folate/20-μg FITC. HeLa cells were incubated with 100-μg/mL of nontargeted nanoshells functionalized with: (d) 9-μg PEG/20-μg FITC, (e) 90-μg PEG/20-μg FITC, (f) 900-μg PEG/20-μg FITC or (g) 20-μg FITC. All cells were stained with Hoescht (blue nuclear dye) and wheat germ agglutinin (WGA, red membrane stain). Folate targeted nanoshells show higher adhesion/endocytosis in HeLa cells compared to their similarly sized PEG counterparts.

background subtraction since the mean red fluorescence intensity was used as an internal control for normalization.

As can be seen in Fig. 7, the fluorescence ratio analysis shows that HeLa cells incubated with folate functionalized nanoshells tend to have larger fluorescence ratios than the corresponding PEG nanoshell samples. The fluorescence ratio values increase significantly as folate concentrations increased, going from a value of 0.34 (SE $\pm$ 0.018) for nanoshells synthesized with 2-μg of folate to 0.77 ($\pm$0.028) for nanoshells synthesized with 200-μg of folate. In contrast, the fluorescence ratio values for increasing PEG samples were constant, ranging from 0.30 ($\pm$0.006) for nanoshells fabricated using 9 μg of PEG to 0.37 ($\pm$0.007) for nanoshells produced using 900 μg of PEG. Moreover, when the fluorescence ratios of folate and their molar equivalent PEG nanoshells counterparts were compared, it was found that folate functionalized nanoshells were always greater than PEG nanoshells. When comparing nanoshells functionalized with 200-μg folate/20-μg FITC to nanoshells coated with 900-μg PEG/20-μg FITC, the fluorescence ratio for folate functionalized nanoshells was 2.1× more intense than their molar equivalent PEG particle counterparts. This suggests that more folate nanoshells adhered to and/or were endocytosed by HeLa cells than their PEG coated counterparts. An unpaired two-tailed *t*-test was performed between folate nanoshells and their PEG molar equivalents. All *t*-tests showed statistical significance (Fig. 7). Since all cell images were obtained with identical microscopy parameters, these results imply that increased nanoshell adhesion/endocytosis by HeLa cells is in part due to their surface modification.

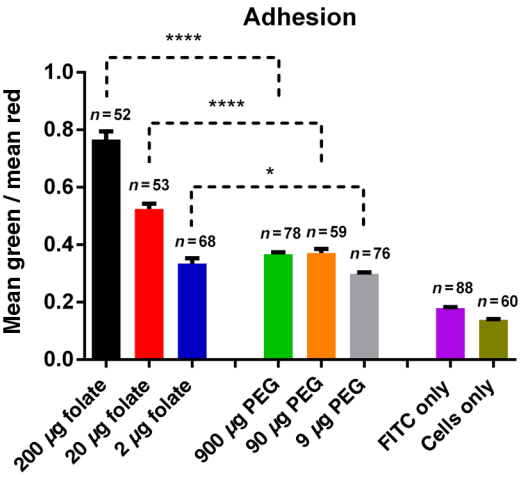

Fig. 7 Fluorescence ratio quantification of nanoshells cell adhesion/endocytosis using fluorescence microscopy images. HeLa cells were incubated with 100 μg/mL of FITC-Nanoshells functionalized with 0, 2, 20, 200 μg folate or 9, 90, 900 μg PEG. Outlines were drawn around each cell membrane stained with red WGA membrane stain. The mean green fluorescence intensity of each outline was collected and divided by the same cell outline mean red fluorescence intensity. This value is represented as fluorescence ratio [$\pm$standard error (SE)]. Nanoshells functionalized with a higher concentration of folate showed higher adhesion and/or endocytosis by HeLa cells. Nanoshells functionalized with PEG showed partial adhesion/endocytosis by HeLa cells. Negligible adhesion/endocytosis for FITC only nanoshells was observed (*significant at $p \leq 0.05$, ****significant at $p \leq 0.0001$, n = number cell outlines in set).

3.4 *Nanoshell Cell Endocytosis Experiments and Confocal Microscopy Image Analysis*

The uptake of nanoshells by HeLa cells was investigated by confocal microscopy. Confocal microscope images were taken of HeLa cancer cells incubated with nanoshells modified with 200-μg folate/20-μg FITC at different z positions: top, inner cut between top and middle slices, and the center cell cut. These confocal images were employed to assess if folate functionalized nanoshells were inside the cells, as opposed to being only on the cell membrane surface.

To characterize folate induced endocytosis, a confocal microscopy comparison was made between folate and PEG functionalized nanoshells. As shown in Fig. 8(a), HeLa cells incubated with folate/FITC functionalized nanoshells show green fluorescence scattered nanoshells within the cytosol region of cells; conversely, HeLa cells treated with plain FITC functionalized nanoshells [Fig. 8(b)] or molar equivalent PEG/FITC coated nanoshells [Fig. 8(c)] exhibited very weak green fluorescence intensities within the confocal image and are similar to control samples of HeLa cells without nanoshells [Fig. 8(d)]. Studies have shown that folic acid-drug conjugates can enhance cancer specificity and in some cases efficacy;[84] however, chemical modification of the drug may affect the drug's intrinsic activity.[85] Therefore, nanoparticle delivery is potentially beneficial since it enables release of a drug in its original, unmodified chemical form.

A modified fluorescence ratio analysis was performed on confocal images by drawing cell outlines around the center cut of individual cells (i.e., z-stack slice with the largest diameter) by using the red membrane cell stain images in order to avoid outlining the same cell more than once throughout the z-stack.

As can be seen in Fig. 9, nanoshells functionalized with increasing amounts of folate have larger fluorescence ratios and their values are much greater than the corresponding PEG functionalized nanoshell samples. The confocal imaging fluorescence ratio values for 200 μg folate targeting nanoshells, 0.81 (SE $\pm$ 0.03), were almost identical to the two-dimensional (2-D) fluorescence microscopy imaging values, 0.77 ($\pm$0.028), implying that most of the 200-μg functionalized nanoshells that adhered to the cells were actually internalized. These results indicate that folate modification not only facilitates the nanoshells to target cancer cell surfaces, but more importantly induces internalization. The fluorescence quantification method described allows for distinction between particle adhesion and internal uptake.

When the confocal fluorescence ratios of folate and their molar equivalent PEG nanoshell counterparts were compared, it was found that folate functionalized nanoshells were always significantly greater than PEG nanoshells. For high-density surface functionalization coatings, the difference in fluorescence ratio were greatest. Nanoshells functionalized with 200-μg folate/20-μg FITC had a 26× greater confocal fluorescence intensity ratio compared to the nanoshells functionalized with 900-μg PEG/20-μg FITC. Note that the confocal fluorescence ratio for PEG functionalized nanoshells is close to that of the cells only samples, so these "x-fold increases" represents a minimum enhancement. An unpaired two-tailed *t*-test was performed between folate nanoshells and their molar equivalent PEG counterparts. All t-tests showed statistical significance (Fig. 9).

As discussed earlier in Fig. 3, the amount of FITC incorporated onto the silica nanoshell surface showed that more FITC was conjugated to the surface of plain and PEG nanoshells

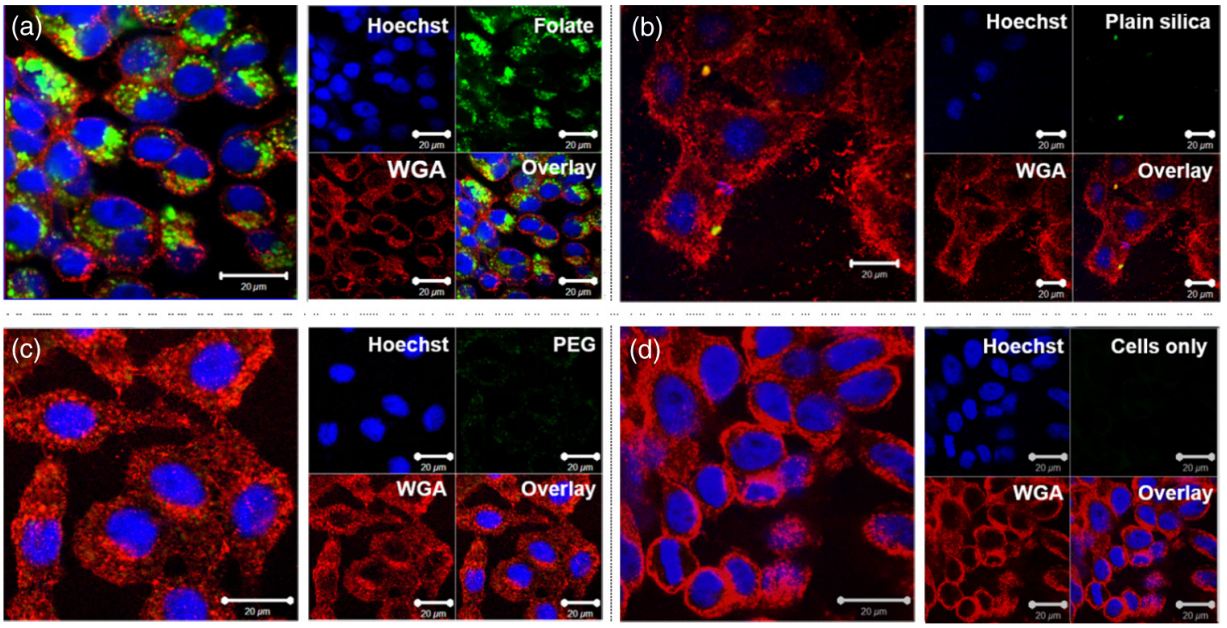

Fig. 8 Confocal microscopy center cross sectional images of HeLa cells incubated with targeted or non-targeted nanoshells. (a) HeLa cells incubated with 100 μg/mL of targeted nanoshells functionalized with 200-μg folate/20-μg FITC; (b) HeLa cells incubated with 100 μg/mL of plain nanoshells 20-μg FITC (c) HeLa cells incubated with 100 μg/mL of nanoshells functionalized with 900-μg PEG/20-μg FITC; (d) HeLa cells only, stained with WGA (red) and Hoechst (blue). Effective cell uptake is observed for folate functionalized nanoshells. Identical settings and gains were used across all microscopy images. A Zeiss LSM510 laser scanning microscope was used to take confocal images.

compared to folate nanoshells, which suggests that the amount of folate-FITC nanoshells internalized may be higher than reported. Furthermore, it is important to note that FITC has an emission quantum yield which is dependent on pH. A dianion, which is present in significant amounts above pH 6, can be about three times more fluorescent than the monoanion and neutral forms of fluorescein.[86,87] Therefore, if the nanoshells are endocytosed and localized in the endosome, the acidic environment of the endosome can decrease the intensity of the particles.[88] For this reason, the reported fluorescence values may further underestimate the amount of endocytosis. In order to avoid this, a non-pH sensitive dye such as rhodamine B isothiocyanate (RITC) can be used as an alternative dye for future studies; it is noted that the cells in this study were imaged postfixation so the differential pH in endosome could be diminished.

These results for 100-nm nanoparticles are supported by a similar study done by Rosenholm et al.,[65] which showed that 400-nm folate targeted mesoporous silica nanoparticles are readily endocytosed by HeLa cells. To reliably distinguish between particle adhesion to the outer part of the membrane and particles internalized by the cells, Rosenholm quenched the extracellular FITC-PEI-folate silica nanoparticles. Their results showed that 48% of the fluorescence signal was lost after quenching, which suggests that about 52% of nanoparticles were effectively endocytosed. Although quenching of fluorophores is a relatively easy method, it is known that the quenching efficiency can vary, quenchers have low specificity, and it can also cause an increase in autofluorescence which can lead to a false positive signal.[89–91] Additionally, trypan blue, which is a typical quencher used for these types of studies, binds to proteins on the cell surface and the resulting complex shifts the green fluorescence to emit in the red channel. For this

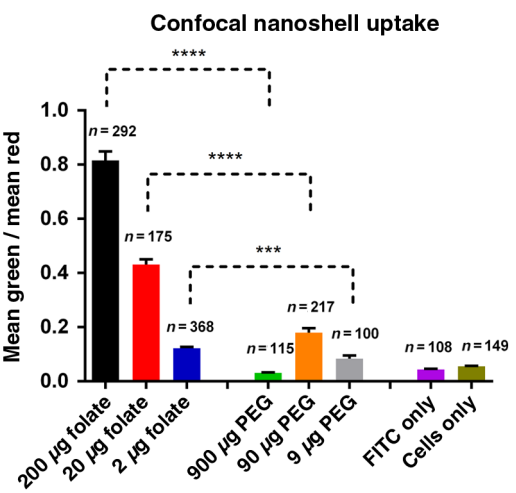

Fig. 9 Quantification of nanoshell cell endocytosis by HeLa cells using confocal cross-sectional image analysis. HeLa cells were incubated with 100 μg/mL of nanoshells with 20 μg of FITC functionalized with 0, 2, 20, 200 μg folate or 9, 90, 900 μg PEG. Using confocal images, cell outlines were only drawn for the slice with largest cell outline diameter which corresponds to the center cut of each individual cell. Cell outlines were based on the cell membranes, which were stained with red Wheat Germ Agglutinin (WGA) dye. The mean green fluorescence intensity of each outline was collected and divided by the same cell outline mean red fluorescence intensity. This value is represented as the confocal fluorescence ratio ($\pm$SE). Folate targeted nanoshells were highly endocytosed by HeLa cells at 20 and 200 μg folate in comparison to their PEG counterparts and nonfunctionalized FITC-nanoshells (***significant at $p \leq 0.001$, ****significant at $p \leq 0.0001$, $n =$ number cell outlines in set).

reason, computation of normalized fluorescence ratios is not the most ideal for the analysis presented in this study.

As discussed above, the present study shows that nearly all the 200-μg folate targeted nanoshells which adhered to the cell surface were effectively endocytosed by the cells as confirmed by confocal microscopy. Quantification of endocytosis using confocal microscopy and the fluorescence ratio analysis described is advantageous since no external quencher is introduced. The higher fraction of endocytosis in the present study compared to the Rosenholm et al.[65] study may be due to the higher surface density of folate and the use of smaller particles (i.e., 100-nm diameter particles compared to 400-nm diameter particles) in the present work among other factors. Several other aspects which may affect the difference in uptake of particles are varying parameters such as particle size and composition, incubation time, particle dose, orientation of folate on the nanoparticle, and type/passage of cell line.

Next, in order to determine the fraction of cells that show any degree of nanoshell endocytosis, the fraction of cells with confocal fluorescence ratios greater than 0.2 were tabulated as shown in Table 3. The largest fluorescence ratio in the cells' only set was found to be 0.1, therefore, in order to have a conservative estimate for positive nanoshell endocytosis a multiple of twice this value was used as a cutoff. Cells with a fluorescence ratio value above 0.2 were considered to be cells demonstrating some type of nanoshell uptake, while cells with a fluorescence ratio below 0.2 were considered to be cells with no nanoshell endocytosis.

As can be seen in Table 3, as folate concentration was increased on the nanoshell surface, the percentage of cells with a fluorescence ratio over the 0.2 cutoff value increased, while only a negligible fraction of the cells incubated with any of the PEG functionalized nanoshells showed internalization. For example, 95% of all HeLa cells incubated with nanoshells functionalized with 200-μg folate/20-μg FITC had a value over the 0.2 cutoff value, implying that these cells had some level of nanoshell endocytosis. Conversely, none of HeLa cells incubated with 900-μg PEG/20-μg FITC had a value above this cutoff, signifying that all the cells in this set did not show particle uptake.

Table 3 Percentage of cells with nanoshell endocytosis using confocal cell outlines. A confocal fluorescence ratio threshold was set at 0.2. This value was chosen to be 2× above the cells only fluorescence ratio maximum which was 0.1. Cells with a fluorescence ratio value above 0.2 were considered to be cells with some nanoshell endocytosis while cells with a fluorescence ratio of value below 0.2 were considered to have no nanoshell endocytosis. Nearly all cells incubated with 20 and 200 μg folate showed nanoshell uptake.

Sample	Number of outlines with value over 0.2[a]	% cells with nanoshell uptake
Cells only	0/0	0%
Cells + 20-μg FITC nanoshells	0/108	0%
Cells + 2-μg folate/20-μg FITC nanoshells	40/368	11%
Cells + 20-μg folate/20-μg FITC nanoshells	157/176	89%
Cells + 200-μg folate/20-μg FITC nanoshells	273/293	95%
Cells + 9-μg PEG/20-μg FITC nanoshells	11/100	11%
Cells + 90-μg PEG/20-μg FITC nanoshells	58/217	27%
Cells + 900-μg PEG/20-μg FITC nanoshells	0/115	0%

[a]Number of cells outlines with a fluorescence value over 0.2 divided by total number cell outlines in set.

3.5 *Nanoshell Selectivity Experiments and Image Analysis*

An important aspect for developing nanoparticles for biomedical applications is their selective targeting. The selectivity properties of folate functionalized nanoshells were studied using a cellular mixture consisting of HeLa cervical cancer cells and normal HFF-1 cells. For this study, only nanoshells functionalized with 200-μg folate/20-μg FITC or 900-μg PEG/20-μg FITC were studied because they showed the most cell interactions in the previous experiments for targeting and nontargeting interactions. As can be seen in Fig. 10, under coculture conditions of HeLa and HFF-1 cells, folate targeted nanoshells almost exclusively adhered to HeLa cells at high numbers, while PEG functionalized nanoshells only bound to a few cells.

The difference in nanoshell cell selectivity between folate and PEG functionalized nanoshells was quantified. Cancer HeLa cells were stained with CMPTX CellTracker red intracellular dye and normal HFF-1 cells were stained with CMAC blue intracellular dye. Due to the use of these dyes, the fluorescence quantification analysis was slightly modified. As depicted in Fig. 10, by using Image J, two different sets of cell outlines were created; one consisting of HeLa cell outlines that were produced using the red channel image and the other for HFF-1 cell outlines produced by using the blue channel image. These sets of outlines were applied to the same location/coordinates on their green channel counterparts by using the ROI manager in Image J. The Image J analyze/measure tools were used to determine the mean green fluorescence values inside each of the individual cell outlines. A background subtraction was applied to each cell outline by subtracting the average mean green fluorescence intensity of their corresponding cells' only sample set (i.e., average mean green fluorescence value of HFF-1 or HeLa only cell sets—while setting any negative values to zero). The mean green fluorescence intensities after background subtraction are referred to as relative mean green fluorescence values from hereon. Finally, these individual relative mean green fluorescence values were averaged for each set. The averaged relative mean green fluorescence values of HeLa cells to HFF-1 cells were compared to each other in each of the cell sample sets (cells incubated with folate functionalized nanoshells and cells incubated with PEG functionalized nanoshells). As shown in Fig. 11, it was found that folate functionalized nanoshells adhered with higher selectivity to HeLa cells rather than to HFF-1 cells by 4.3×. The uptake levels of folate functionalized nanoshells in normal HFF-1 cells are similar to the low-uptake levels of nontargeted PEG nanoshells. A two way ANOVA was performed on this data set and all showed statistical significance (Fig. 11). These findings indicate that folate functionalized nanoshells are selective toward HeLa cancer cells with negligible nonspecific binding or uptake by HFF normal cells.

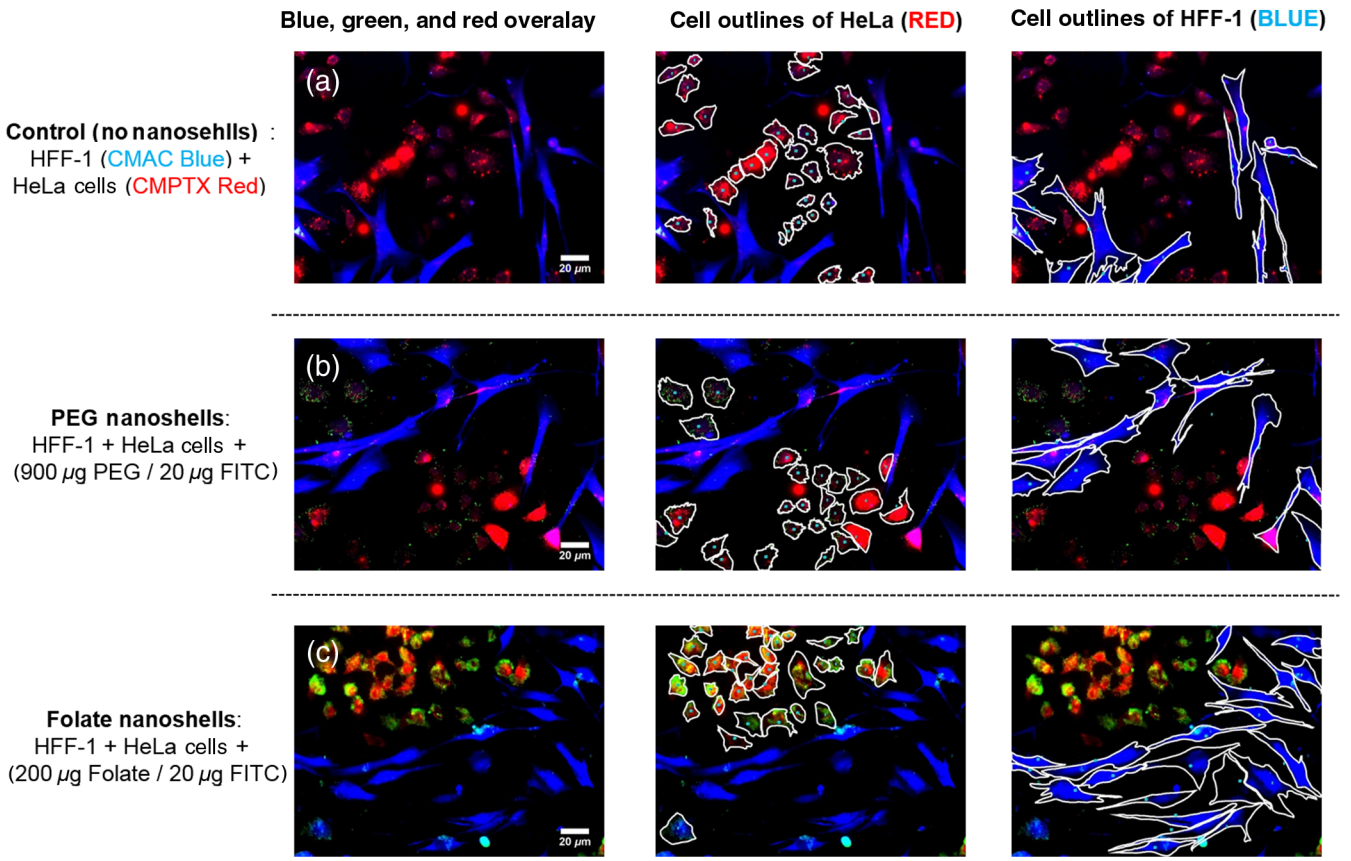

Fig. 10 Comparison of Selectivity of nontargeted and targeted nanoshells in coculture of HeLa and HFF-1 cells using fluorescence microscopy. (a) Coculture of HeLa cancer cells, stained with CMPTX (red), and normal human foreskin fibroblast (HFF-1), stained with CMAC (blue); (b) HeLa and HFF-1 cells incubated with 50 μg/mL of nontargeted nanoshells functionalized with 900-μg PEG/20-μg FITC; (c) HeLa and HFF-1 cells incubated with 50 μg/mL of targeted nanoshells functionalized with 200-μg folate/20-μg FITC. Folate functionalized FITC-nanoshells show to be highly selective for HeLa cancer cells compared to normal HFF-1 cells. White markings are cell outlines used to quantify nanoshells cell selectivity.

4 Conclusions

A simple fluorescence ratio analysis was developed in order to quantify and distinguish endocytosis versus cell adhesion. Hollow silica nanoshells functionalized with FITC and folate were synthesized and used as a targeting nanoparticle platform. The quantification method showed that folate functionalized SiO_2 nanoshells bound to HeLa cervical cancer cells by a factor of 2.1× more than PEG functionalized silica nanoshells. The confocal fluorescence ratio analysis was consistent with roughly 26× more folate functionalized nanoshells being endocytosed by HeLa cells compared to the internalization of similar nontargeted PEG nanoshells. Comparison between the fluorescence ratios from the 2-D and three-dimensional (3-D) fluorescence imaging shows nearly all the folate functionalized silica nanoshells were endocytosed, while a negligible amount of PEG functionalized nanoshells were endocytosed. Under HeLa/HFF-1 coculture conditions, folate nanoshells were found to be selectively bound to HeLa cancer cells by a factor of 4.3×. The efficient internalization and selective properties of folate functionalized nanoshells make these particles promising candidates for selective targeted drug delivery. Furthermore, it has been shown that a fluorescence ratio analysis, when used in conjunction with 2-D fluorescence and 3-D confocal microscopy, can be a quick method to distinguish nanoparticle surface adhesion from nanoparticle internalization and can also quantify these parameters. The fluorescence ratio analysis described is a simple quantification method which can potentially eliminate the need for multiple washes and lysing steps, as well as the need to use multiple analytical techniques, to define nanoparticle-cell interactions.

Appendix

1. Calculation of weight factor

$$V_{\text{solid}} = \frac{4}{3}\pi r_{\text{solid}}^3.$$

$$V_{\text{shell}} = \frac{4}{3}\pi r_{\text{solid}}^3 - \frac{4}{3}\pi r_{\text{inner hollow radius}}^3.$$

$$\text{Weight fraction} = \frac{V_{\text{shell}}}{V_{\text{solid}}} = \frac{r_{\text{shell}}^3 - r_{\text{solid}}^3}{r_{\text{solid}}^3}.$$

$$\text{WF}_{100\text{ nm nanoshell}} = \frac{(50^3\text{ nm}) - (40^3\text{ nm})}{(50^3\text{ nm})} = 0.488.$$

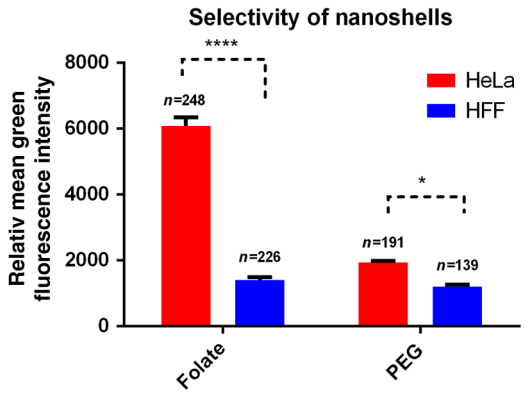

Fig. 11 Two-dimensional (2-D) quantification of nanoshells cell adhesion/endocytosis selectivity by fluorescence microscopy. Cocultures of Hela cells and HFF-1 cells were incubated with 50 μg/mL of nanoshells with 20 μg of FITC functionalized with 200-μg folate or 900-μg PEG. HeLa cancer cells were stained with red CMPTX dye, and normal human foreskin fibroblast (HFF-1) were stained with blue CMAC dye. Outlines were drawn around the cell membranes and the mean green fluorescence intensity of each cell outline was collected for HeLa and HFF-1 cells. A background subtraction was applied to each individual cell outline by subtracting the average mean green fluorescence intensity of the corresponding cells only sample set (i.e., HeLa or HFF-1 cells only outlines), shown as relative mean green fluorescence (±SE). Folate targeted FITC-nanoshells showed significant selectivity for HeLa cancer cells compared to HFF-1 normal cells. PEG targeted FITC-nanoshells showed little adhesion/endocytosis by both HeLa and HFF-1 cells (*significant at $p \leq 0.05$, ****significant at $p \leq 0.0001$, $n =$ number cell outlines in set). Quantification was performed on 2-D fluorescence images.

2. Mass of one hollow nanoshell (NS)

$$m_{\text{solid nanoshell}} = V_{\text{solid}} \times \rho_{\text{amorphous silica}} = \frac{4}{3}\pi(50\text{ nm})^3 \times 2.28\text{ g/cm}^3 = 1.19 \times 10^{-15}\text{ g}.$$

$$m_{\text{hollow nanoshell}} = \text{WF} \times m_{\text{solid nanoshell}} = 0.488 \times 1.19 \times 10^{-15}\text{ g} = 5.81 \times 10^{-16}\text{ g/NS}.$$

Density of amorphous silica is given in Ref. 92.

3. Number of hollow nanoshells (NS) in 3 mg

$$3\text{ mg of nanoshells} \times \frac{1\text{ g}}{1000\text{ mg}} \times \frac{1\text{ NS}}{5.81 \times 10^{-16}\text{ g}} = 5.16 \times 10^{12}\text{ NS}.$$

4. Number of folate molecules on a nanoshell (on surface and core)

Calculated using UV Vis data for nanoshells coated with only 200-μg folate:

3.47×10^{16} folate molecules/3 mg of NS.

Therefore,

$$\frac{3.47 \times 10^{16}\text{ folate molecules}}{3\text{ mg of NS}} \times \frac{3\text{ mg of NS}}{5.16 \times 10^{12}\text{ NS}} = 6.72 \times 10^{3}\text{ folate molecules / NS}.$$

5. Calculation of surface area factor (SAF)

$$\text{Surface Area (SA) of hollow NS (based on BET data)} = 400\,\text{m}^2/\text{g}.$$

$$\text{Total SA (on surface and core of one hollow NS)} = \frac{400\text{ m}^2}{\text{g}} \times \frac{5.81 \times 10^{-16}\text{ g}}{1\text{ NS}} = 2.32 \times 10^{-13}\text{ m}^2.$$

$$\text{Outer SA of one hollow NS} = 4\pi r^2 = 4\pi(50\text{ nm})^2 = 3.14 \times 10^{-14}\text{ m}^2.$$

$$\text{SAF} = \frac{\text{Outer nanoshell SA}}{\text{Total SA of Porous Hollow NS}} = \frac{3.14 \times 10^{-14}\text{ m}^2}{2.32 \times 10^{-13}\text{ m}^2} = 0.135.$$

6. Number of folate molecules per nm^2 on total NS surface area

$$\frac{\text{Number of Folate Molecules}}{\text{Total Surface Area BET}_{\text{Data}}} = \frac{6.72 \times 10^{3}\text{ Folate molecules}}{\text{NS}} \times \frac{\text{NS}}{2.32 \times 10^{-13}\text{ m}^2} = \frac{2.90 \times 10^{16}\,\text{Folate molecules}}{\text{m}^2} = \frac{2.90 \times 10^{-2}\,\text{Folate molecules}}{\text{nm}^2}.$$

7. Number of folate molecules on outer surface per NS

$$\text{Number of folate molecules on outer surface per NS} = \frac{6.72 \times 10^{3}\,\text{Folate molecules}}{\text{NS}} \times 0.135 = \frac{9.07 \times 10^{2}\,\text{Folate molecules}}{\text{NS}}.$$

Equations: example calculations of weight factor, mass of single nanoshell (NS), and estimate of maximum amount of folate molecules on the surface of one nanoshell. The weight factor equation allows for a reasonable mass estimation of a hollow particle. The weight factor was determined by subtracting the internal volume of a nanoshell using the inner and outer radius that we calculated from our previous work. This ratio also

allowed us to estimate the mass of an individual nanoshell, which we consequently used to calculate the number of nanoshells in a given mass and the maximum amount of folate molecules on the surface of one nanoshell based on UV-Vis collected data.

Acknowledgments

This research was supported by NIH Nanotumor Grant (NIH Grant U54 CA 119335), Samsung GRO Grant, NIH IMAT 1R33CA177449-01A1, and we thank the California Institute of Information Technology and Telecommunication and the Air Force Office of Scientific Research (AFOSR grant number FA9550-12-1-0381) for research support. In addition, individual student funding was provided by NIH Ruth L. Kirschstein National Research Service Award F31 Fellowship (NIH Grant No. 5F31 EB010375), NCI Research Supplements to Promote Diversity in Health Related Research Fellowship (NIH Grant No. 3U54 CA 119335-05S3), NSF—California LSAMP Bridge to the Doctorate/Louis Stokes Alliances for Minority Participation Fellowship (UCINSF Grant No. HRD0115115), NIH—ET CURE/Specialized Cancer Center Support (NIH Grant No. 3P30 CA 023100–25S7), and the NIH—Cross Training Translation Cancer Researchers in Nanotechnology (CRIN) Support (NIH Grant No. 3 R25 CA 153915-03S1). Dr. Kersi Pestonjamasp and the rest of the Cancer Center Microscopy Core Facility at UCSD (NCI Grant No. P30 CA23100) is acknowledged for assistance in obtaining the confocal images. Norm Olson and the Timothy S. Baker Cryoelectron Microscopy Laboratory are acknowledged for assistance in obtaining the transmission electron microscopy images. S.S. conceived the experiments; S.S., J.Y., S.A. designed the experiments, S.S., J.G.A, S.A, and A.L. performed the experiments; S.S., N.M., J.G.A analyzed the data. S.S., N.M., A.L., W.C.T, and A.C.K. cowrote the paper.

References

1. J. M. Chan et al., "PLGA-lecithin-PEG coreshell nanoparticles for controlled drug delivery," *Biomaterials* **30**(8), 1627–1634 (2009).
2. J. Cheng et al., "Formulation of functionalized PLGA-PEG nanoparticles for *in vivo* targeted drug delivery," *Biomaterials* **28**(5), 869–876 (2007).
3. A. E. de Salamanca et al., "Chitosan nanoparticles as a potential drug delivery system for the ocular surface: toxicity, uptake mechanism and *in vivo* tolerance," *Invest. Ophthalmol. Visual Sci.* **47**(4), 1416–1425 (2006).
4. M. E. Davis, "The first targeted delivery of siRNA in humans via a self-assembling, cyclodextrin polymer-based nanoparticle: from concept to clinic," *Mol. Pharmaceutics* **6**(3), 659–668 (2009).
5. G. Kong et al., "Efficacy of liposomes and hyperthermia in a human tumor xenograft model: importance of triggered drug release," *Cancer Res.* **60**(24), 6950–6957 (2000).
6. S. Ibsen et al., "A novel nested liposome drug delivery vehicle capable of ultrasound triggered release of its payload," *J. Controlled Release* **155**(3), 358–366 (2011).
7. A. Bandekar et al., "Antitumor efficacy following the intracellular and interstitial release of liposomal doxorubicin," *Biomaterials* **33**(17), 4345–4352 (2012).
8. M. S. Muthu et al., "Theranostic liposomes of TPGS coating for targeted co-delivery of docetaxel and quantum dots," *Biomaterials* **33**(12), 3494–3501 (2012).
9. S. D. Kong et al., "Magnetically vectored nanocapsules for tumor penetration and remotely switchable on-demand drug release," *Nano Lett.* **10**(12), 5088–5092 (2010).
10. J. Yang, J. U. Lind, and W. C. Trogler, "Synthesis of hollow silica and titania nanospheres," *Chem. Mater.* **20**(9), 2875–2877 (2008).
11. P. Podsiadlo et al., "Gold nanoparticles enhance the anti-leukemia action of a 6-mercaptopurine chemotherapeutic agent," *Langmuir* **24**(2), 568–574 (2008).
12. A. K. Gupta and M. Gupta, "Synthesis and surface engineering of iron oxide nanoparticles for biomedical applications," *Biomaterials* **26**(18), 3995–4021 (2005).
13. O. M. Koo, I. Rubinstein, and H. Onyuksel, "Role of nanotechnology in targeted drug delivery and imaging: a concise review," *Nanomed. Nanotechnol. Biol. Med.* **1**(3), 193–212 (2005).
14. H. Gelderblom et al., "Cremophor EL: the drawbacks and advantages of vehicle selection for drug formulation," *Eur. J. Cancer* **37**(13), 1590–1598 (2001).
15. M. A. Behlke, "Progress towards *in vivo* use of siRNAs," *Mol. Ther.* **13**(4), 644–670 (2006).
16. K. S. Chu et al., "Nanoparticle drug loading as a design parameter to improve docetaxel pharmacokinetics and efficacy," *Biomaterials* **34**(33), 8424–8429 (2013).
17. T. Paunesku et al., "Biology of TiO_2-oligonucleotide nanocomposites," *Nat. Mater.* **2**(5), 343–346 (2003).
18. J. M. Caster et al., "Nanoparticle delivery of chemosensitizers improve chemotherapy efficacy without incurring additional toxicity," *Nanoscale* **7**(6), 2805–2811 (2015).
19. J. D. Rocca et al., "Polysilsesquioxane nanoparticles for triggered release of cisplatin and effective cancer chemoradiotherapy," *Nanomed. Nanotechnol. Biol. Med.* **11**(1), 31–38 (2015).
20. A. Z. Wang, R. Langer, and O. C. Farokhzad, "Nanoparticle delivery of cancer drugs," *Annu. Rev. Med.* **63**, 185–198 (2012).
21. F. Chen, E. B. Ehlerding, and W. Cai, "Theranostic nanoparticles," *J. Nucl. Med.* **55**(12), 1919–1922 (2014).
22. F. Chen et al., "*In vivo* tumor targeting and image-guided drug delivery with antibody-conjugated, radiolabeled mesoporous silica nanoparticles," *ACS Nano* **7**(10), 9027–9039 (2013).
23. M.-Y. Chang, J. Seideman, and S. Sofou, "Enhanced loading efficiency and retention of 225Ac in rigid liposomes for potential targeted therapy of micrometastases," *Bioconjugate Chem.* **19**(6), 1274–1282 (2008).
24. S. A. Kularatne and P. S. Low, "Targeting of nanoparticles: folate receptor," *Methods Mol. Biol.* **624**, 249–265 (2010).
25. I. G. Campbell et al., "Folate-binding protein is a marker for ovarian-cancer," *Cancer Res.* **51**(19), 5329–5338 (1991).
26. S. D. Weitman et al., "Distribution of the folate receptor Gp38 in normal and malignant-cell lines and tissues," *Cancer Res.* **52**(12), 3396–3401 (1992).
27. S. D. Weitman, K. M. Frazier, and B. A. Kamen, "The folate receptor in central-nervous-system malignancies of childhood," *J. Neuro-Oncol.* **21**(2), 107–112 (1994).
28. G. Toffoli et al., "Overexpression of folate binding protein in ovarian cancers," *Int. J. Cancer* **74**(2), 193–198 (1997).
29. J. Holm et al., "Characterization of a high-affinity folate receptor in normal and malignant human testicular tissue," *Biosci. Rep.* **19**(6), 571–580 (1999).
30. J. F. Ross et al., "Folate receptor type beta is a neutrophilic lineage marker and is differentially expressed in myeloid leukemia," *Cancer* **85**(2), 348–357 (1999).
31. R. Bueno et al., "The alpha folate receptor is highly activated in malignant pleural mesothelioma," *J. Thorac. Cardiovasc. Surg.* **121**(2), 225–233 (2001).
32. J. Shia et al., "Immunohistochemical expression of folate receptor α in colorectal carcinoma: patterns and biological significance," *Hum. Pathol.* **39**(4), 498–505 (2008).
33. J. Sudimack and R. J. Lee, "Targeted drug delivery via the folate receptor," *Adv. Drug Delivery Rev.* **41**(2), 147–162 (2000).
34. P. Garinchesa et al., "Trophoblast and ovarian-cancer antigen-Lk26-sensitivity and specificity in immunopathology and molecular-identification as a folate-binding protein," *Am. J. Pathol.* **142**(2), 557–567 (1993).
35. X. Wang et al., "Differential stereospecificities and affinities of folate receptor isoforms for folate compounds and antifolates," *Biochem. Pharmacol.* **44**(9), 1898–1901 (1992).
36. Y. J. Lu et al., "Folate receptor-targeted immunotherapy of cancer: mechanism and therapeutic potential," *Adv. Drug Delivery Rev.* **56**(8), 1161–1176 (2004).

37. Y. J. Lu and P. S. Low, "Folate-mediated delivery of macromolecular anticancer therapeutic agents," *Adv. Drug Delivery Rev.* **54**(5), 675–693 (2002).
38. L. Brannon-Peppas and J. O. Blanchette, "Nanoparticle and targeted systems for cancer therapy," *Adv. Drug Delivery Rev.* **56**(11), 1649–1659 (2004).
39. J. F. Ross, P. K. Chaudhuri, and M. Ratnam, "Differential regulation of folate receptor isoforms in normal and malignant tissues *in vivo* and in established cell lines. Physiologic and clinical implications," *Cancer* **73**(9), 2432–2443 (1994).
40. H. Hong et al., "*In vivo* targeting and imaging of tumor vasculature with radiolabeled, antibody-conjugated nanographene," *ACS Nano* **6**(3), 2361–2370 (2012).
41. L. Brannon-Peppas and J. O. Blanchette, "Nanoparticle and targeted systems for cancer therapy," *Adv. Drug Delivery Rev.* **64**, 206–212 (2012).
42. M. E. Davis, Z. Chen, and D. M. Shin, "Nanoparticle therapeutics: an emerging treatment modality for cancer," *Nat. Rev. Drug Discovery* **7**(9), 771–782 (2008).
43. J. D. Byrne, T. Betancourt, and L. Brannon-Peppas, "Active targeting schemes for nanoparticle systems in cancer therapeutics," *Adv. Drug Delivery Rev.* **60**(15), 1615–1626 (2008).
44. F. X. Gu et al., "Targeted nanoparticles for cancer therapy," *Nano Today* **2**(3), 14–21 (2007).
45. Y. Zhang, N. Kohler, and M. Q. Zhang, "Surface modification of superparamagnetic magnetite nanoparticles and their intracellular uptake," *Biomaterials* **23**(7), 1553–1561 (2002).
46. M. O. Oyewumi and R. J. Mumper, "Influence of formulation parameters on gadolinium entrapment and tumor cell uptake using folate-coated nanoparticles," *Int. J. Pharm.* **251**(1–2), 85–97 (2003).
47. J. F. Kukowska-Latallo et al., "Nanoparticle targeting of anticancer drug improves therapeutic response in animal model of human epithelial cancer," *Cancer Res.* **65**(12), 5317–5324 (2005).
48. S. A. Kularatne and P. S. Low, "Targeting of nanoparticles: folate receptor," *Methods Mol. Biol.* **624**, 249–265 (2010).
49. J. M. Rosenholm et al., "Targeted intracellular delivery of hydrophobic agents using mesoporous hybrid silica nanoparticles as carrier systems," *Nano Lett.* **9**(9), 3308–3311 (2009).
50. I. Slowing, B. G. Trewyn, and V. S.-Y. Lin, "Effect of surface functionalization of MCM-41-type mesoporous silica nanoparticles on the endocytosis by human cancer cells," *J. Am. Chem. Soc.* **128**(46), 14792–14793 (2006).
51. Q. Zhang et al., "Multifunctional mesoporous silica nanoparticles for cancer-targeted and controlled drug delivery," *Adv. Funct. Mater.* **22**(24), 5144–5156 (2012).
52. I. Hussain et al., "Size-controlled synthesis of near-monodisperse gold nanoparticles in the 1–4 nm range using polymeric stabilizers," *J. Am. Chem. Soc.* **127**(47), 16398–16399 (2005).
53. P. Nativo, I. A. Prior, and M. Brust, "Uptake and intracellular fate of surface-modified gold nanoparticles," *ACS Nano* **2**(8), 1639–1644 (2008).
54. W. Cai et al., "Applications of gold nanoparticles in cancer nanotechnology," *Nanotechnol. Sci Appl.* **2008**(1) (2008).
55. M. Brust and C. J. Kiely, "Some recent advances in nanostructure preparation from gold and silver particles: a short topical review," *Colloids Surf. A* **202**(2), 175–186 (2002).
56. X.-H. Peng et al., "Targeted magnetic iron oxide nanoparticles for tumor imaging and therapy," *Inter. J. Nanomed.* **3**(3), 311–321 (2008).
57. A. Gabizon et al., "Tumor cell targeting of liposome-entrapped drugs with phospholipid-anchored folic acid-PEG conjugates," *Adv. Drug Delivery Rev.* **56**(8), 1177–1192 (2004).
58. C. P. Leamon, S. R. Cooper, and G. E. Hardee, "Folate-liposome-mediated antisense oligodeoxynucleotide targeting to cancer cells: evaluation in vitro and *in vivo*," *Bioconjugate Chem.* **14**(4), 738–747 (2003).
59. V. P. Torchilin, "Recent advances with liposomes as pharmaceutical carriers," *Nat. Rev. Drug Discovery* **4**(2), 145–160 (2005).
60. S. Karve et al., "The pH-dependent association with cancer cells of tunable functionalized lipid vesicles with encapsulated doxorubicin for high cell-kill selectivity," *Biomaterials* **31**(15), 4409–4416 (2010).
61. S. Karve et al., "The use of pH-triggered leaky heterogeneities on rigid lipid bilayers to improve intracellular trafficking and therapeutic potential of targeted liposomal immunochemotherapy," *Biomaterials* **30**(30), 6055–6064 (2009).
62. L. Zhang et al., "Self-assembled lipid-polymer hybrid nanoparticles: a robust drug delivery platform," *ACS Nano* **2**(8), 1696–1702 (2008).
63. X. Shi et al., "Dendrimer-entrapped gold nanoparticles as a platform for cancer-cell targeting and imaging," *Small* **3**(7), 1245–1252 (2007).
64. J. E. Rosen et al., "Iron oxide nanoparticles for targeted cancer imaging and diagnostics," *Nanomed. Nanotechnol. Biol. Med.* **8**(3), 275–290 (2012).
65. J. M. Rosenholm et al., "Targeting of porous hybrid silica nanoparticles to cancer cells," *ACS Nano* **3**(1), 197–206 (2009).
66. W. Zauner, N. A. Farrow, and A. M. R. Haines, "In vitro uptake of polystyrene microspheres: effect of particle size, cell line and cell density," *J. Controlled Release* **71**(1), 39–51 (2001).
67. K. T. Thurn et al., "Endocytosis of titanium dioxide nanoparticles in prostate cancer PC-3M cells," *Nanomed. Nanotechnol. Biol. Med.* **7**(2), 123–130 (2011).
68. F. X. Hu, K. G. Neoh, and E. T. Kang, "Synthesis and in vitro anticancer evaluation of tamoxifen-loaded magnetite/PLLA composite nanoparticles," *Biomaterials* **27**(33), 5725–5733 (2006).
69. J. Davda and V. Labhasetwar, "Characterization of nanoparticle uptake by endothelial cells," *Int. J. Pharm.* **233**(1–2), 51–59 (2002).
70. C. R. Miller et al., "Liposome-cell interactions in vitro: effect of liposome surface charge on the binding and endocytosis of conventional and sterically stabilized liposomes," *Biochemistry* **37**(37), 12875–12883 (1998).
71. B. D. Chithrani, A. A. Ghazani, and W. C. W. Chan, "Determining the size and shape dependence of gold nanoparticle uptake into mammalian cells," *Nano Lett.* **6**(4), 662–668 (2006).
72. K. Y. Win and S.-S. Feng, "Effects of particle size and surface coating on cellular uptake of polymeric nanoparticles for oral delivery of anticancer drugs," *Biomaterials* **26**(15), 2713–2722 (2005).
73. A. Liberman et al., "Hollow silica and silica-boron nano/microparticles for contrast-enhanced ultrasound to detect small tumors," *Biomaterials* **33**(20), 5124–5129 (2012).
74. H. P. Martinez et al., "Hard shell gas-filled contrast enhancement particles for colour Doppler ultrasound imaging of tumors," *MedChemComm* **1**(4), 266–270 (2010).
75. W. C. Trogler et al., *Hollow Silica Nanospheres for Drug Delivery and Gene Transfer*, U.S. Patent No. 8,440,229 (2013).
76. Y. Song et al., "Fluorescent carbon nanodots conjugated with folic acid for distinguishing folate-receptor-positive cancer cells from normal cells," *J. Mater. Chem.* **22**(25), 12568–12573 (2012).
77. R. Schneider et al., "Design, synthesis, and biological evaluation of folic acid targeted tetraphenylporphyrin as novel photosensitizers for selective photodynamic therapy," *Bioorg. Med. Chem.* **13**(8), 2799–2808 (2005).
78. L. Xiong et al., "Synthesis of ligand-functionalized water-soluble [18 F] YF 3 nanoparticles for PET imaging," *Nanoscale* **5**(8), 3253–3256 (2013).
79. J. Yang et al., "Hollow silica nanospheres containing a silafluorene-fluorene conjugated polymer for aqueous TNT and RDX detection," *Chem. Commun.* **46**(36), 6804–6806 (2010).
80. K. K. Pohaku Mitchell et al., "Iron(III)-doped, silica nanoshells: a biodegradable form of silica," *J. Am. Chem. Soc.* **134**(34), 13997–14003 (2012).
81. M. Ogris et al., "DNA/polyethylenimine transfection particles: Influence of ligands, polymer size, and PEGylation on internalization and gene expression," *AAPS PharmSci* **3**(3), 43–53 (2001).
82. S. Mishra, P. Webster, and M. E. Davis, "PEGylation significantly affects cellular uptake and intracellular trafficking of non-viral gene delivery particles," *Eur. J. Cell Biol.* **83**(3), 97–111 (2004).
83. J. Yang et al., "Red-luminescent europium (III) doped silica nanoshells: synthesis, characterization, and their interaction with HeLa cells," *J. Biomed. Opt.* **16**(6), 066012 (2011).
84. C. A. Ladino et al., "Folate-maytansinoids: target-selective drugs of low molecular weight," *Int. J. Cancer* **73**(6), 859–864 (1997).
85. C. P. Leamon and J. A. Reddy, "Folate-targeted chemotherapy," *Adv. Drug Delivery Rev.* **56**(8), 1127–1141 (2004).
86. N. Klonis and W. H. Sawyer, "Spectral properties of the prototropic forms of fluorescein in aqueous solution," *J. Fluoresc.* **6**(3), 147–157 (1996).
87. R. Sjöback, J. Nygren, and M. Kubista, "Absorption and fluorescence properties of fluorescein," *Spectrochim. Acta Part A* **51**(6), L7–L21 (1995).

88. Y.-P. Chen et al., "Surface charge effect in intracellular localization of mesoporous silica nanoparticles as probed by fluorescent ratiometric pH imaging," *Rsc Adv.* **2**(3), 968–973 (2012).
89. E. S. Van Amersfoort and J. A. Van Strijp, "Evaluation of a flow cytometric fluorescence quenching assay of phagocytosis of sensitized sheep erythrocytes by polymorphonuclear leukocytes," *Cytometry* **17**(4), 294–301 (1994).
90. H. Liu and A. P. R. Johnston, "A programmable sensor to probe the internalization of proteins and nanoparticles in live cells," *Angew. Chem. Int. Ed.* **52**(22), 5744–5748 (2013).
91. K. Liang et al., "Endocytic capsule sensors for probing cellular internalization," *Adv. Healthcare Mater.* **3**(10), 1551–1554 (2014).
92. S. Braunauer, D. L. Kantro, and C. H. Weise, "The surface energies of amorphous silica and hydrous amorphous silica," *Can. J. Chem.* **34**, 1483–1496 (1956).

Sergio Sandoval received his PhD in bioengineering in 2012 from the University of California, San Diego (UCSD), where his thesis focused on developing silica, titania, and polymer-hybrid nanoparticle platforms for cancer therapy and diagnostic purposes. Currently, he is a postdoctoral scholar in UCSD's Electrical Engineering Department, where he is developing cleanroom protocols to modify microchips for use in measuring total alkalinity in sea water during deep sea exploration.

William C. Trogler is a professor of chemistry at UCSD. Honors include Phi Beta Kappa, Alfred P. Sloan research fellowship, and fellow of American Association for the Advancement of Science. He has published over 200 research papers, 11 patent disclosures, and two books (one edited). In recent years, his research interests have centered on luminescent polymer sensors for explosives, chemical sensors, and biomedical applications of nanoparticles.

Andrew C. Kummel is a professor in the Department of Chemistry and Biochemistry at UCSD, an affiliated faculty member in nanoengineering as well as materials science and engineering, and the assistant director of the UCSD Moores Cancer Center for Engineering and Physical Sciences. He is the author of over 160 papers on the topics of surface chemistry, ultramicroscopy, and synthesis of silica nanoshells for tumor ultrasound imaging and ablation.

Biographies for the other authors are not available.